Environmental Science Nano

ROYAL SOCIETY OF CHEMISTRY

PAPER

View Article Online
View Journal | View Issue

Check for updates

Cite this: *Environ. Sci.: Nano*, 2021, **8**, 174

Smart nanocomposites of chitosan/alginate nanoparticles loaded with copper oxide as alternative nanofertilizers†

Marco Leonardi, [a] Giuseppe M. Caruso,[ab] Sabrina C. Carroccio, [ac] Simona Boninelli,[d] Giusy Curcuruto,[c] Massimo Zimbone,[a] Maria Allegra,[e] Biagio Torrisi,[e] Filippo Ferlito[e] and Maria Miritello *[a]

Received 30th July 2020,
Accepted 12th October 2020

DOI: 10.1039/d0en00797h

rsc.li/es-nano

In order to best nutrient use efficiency, as required by the increasing food demand for the future global population, in this work an innovative hybrid nanocomposite was designed as an alternative nanoscale fertilizer. An environmentally friendly chemical preparation based on polyelectrolyte complexation was used. A chitosan and sodium alginate complex was selected as a biodegradable shell to release the nanoscale nutrient, CuO nanoparticles. By optimizing the synthesis conditions, *i.e.* pH and polymer/cross-linker ratio, good stability and accurate size control of the resulting nanocomposites were achieved. The morphology features were evaluated using scanning and transmission electron microscopy, and chemical characterization was performed using X-ray diffraction, thermogravimetric analysis, Fourier-transform infrared spectroscopy, dynamic light scattering and inductively coupled plasma optical emission spectrometry. All the collected data confirmed spontaneous polymeric aggregation in nanostructures of sperical shape, having a mean diameter of about 300 nm, as well as CuO encapsulation inside the polymeric coating. Moreover, the role of the biopolymer shell in the significant slowing of copper release from the hybrid nanocomposite was reported. Finally, the nanocomposite efficacy in seeding and germination was evaluated on *Fortunella margarita* Swingle seeds. The tests demonstrated the benefits in the seedling growth together with a synergic effect in developing both the epigean and hypogean parts. The obtained results indicated that the proposed hybrid nanocomposite could be a potential alternative to realize a smart delivery nanofertilizer using an eco-sustainable method.

Environmental significance

The emergent increase in global food demand is a direct consequence of the growth in the world population. To address this issue, mass fertilization is used, but inefficient plant nutrition is still an issue and there are important environmental drawbacks to this process. Herein, an innovative nanofertilizer is proposed, a hybrid nanocomposite mainly made up of chitosan and alginate loaded with copper oxide nanoparticles, prepared using an environmentally friendly and ecosustainable method. A biopolymer shell enhances the adhesion of the material to leaves and protects the nutrients from degradation, limiting the loss of chemicals and slowing the nutrient release. Thus, the developed approach both avoids undesired accumulation in soil and increases nutrient use efficacy.

Introduction

In 2050 the world population is estimated to reach 10 billion people, and a simultaneous increase in global food demand is predicted. This scenario would require the extension of arable land,[1] but currently 37% of the land is already dedicated to agriculture and no more is available because of soil degradation (erosion, mineral deficiency, drought and salinity) and competition with industry and municipalities. However, the current methods of cultivation are known not be efficient enough to address the estimated food demand; nowadays around 50% of used fertilizers are not taken up by

[a] *CNR-IMM, Via Santa Sofia 64, I-95123 Catania, Italy. E-mail: maria.miritello@ct.infn.it*
[b] *CSFNSM, Via S. Sofia 64 - 95123, CATANIA, Italy*
[c] *CNR-IPCB, Via Paolo Gaifami 18, I-95126, Catania, Italy*
[d] *CNR-IMM, Via VIII Strada Z. I. 5, I-95121 Catania, Italy*
[e] *CREA, Consiglio per la ricerca in agricoltura e l'analisi dell'economia agraria, Centro di ricerca Olivicoltura, Frutticoltura e Agrumicoltura, Corso Savoia 190, 95024 Acireale (CT), Italy*

† Electronic supplementary information (ESI) available. See DOI: 10.1039/d0en00797h

plants, but instead lost in the soil, causing collateral environmental impact such as water eutrophication, groundwater poisoning and greenhouse gas production.[2] Their impact on the environment is further increased if they are based on essential micronutrients such as copper, since this element is also used for the control of plant fungal disease. As far as this micronutrient is concerned, elevated concentrations of Cu are toxic towards normal plant development.[3] Indeed, Cu affects metabolic reactions and plays a key role in several physiological processes, such as photosynthesis, respiration, carbohydrate distribution and protein metabolism,[4] but an excess of this element has negative effects, resulting in leaf chlorosis,[5] reduction in root growth and exploration,[6,7] reduction in net photosynthesis[8] and, in some cases, tissue necrosis and plant death.[9] Copper toxicity starts when it is accumulated in the cells and arises due to oxidative stress as a result of the increase in the reactive oxygen species levels, such as superoxide anion (O_2^-), singlet oxygen ($^1O_2$), hydrogen peroxide (H_2O_2) and hydroxyl radical ($^{\cdot}OH^-$).[6,10] On the contrary, under severe Cu deficiency, die-back of stems has been observed in trees. In particular, in citrus this has been verified in nursery by the formation of gum pockets in new branches resulting from tissue breaking down and consequent sap leakage from the xylem and phloem vessels.[11] In non-bearing trees, these symptoms are characterized by the growth of branches that curve in an "S" shape, excessive development of leaf blades and protruding veins on their underside.[12] Therefore, the importance of controlling fertilizer input and increasing uptake efficacy is evident.

In order to address these issues, nanotechnology has been explored[1] in recent years, for example by realizing nanostructured biosensors for the real-time detection of plant health status and for the controlled distribution of bioactive fertilizer compounds[2] and by developing novel nanoscale fertilizers.[13] A nanofertilizer refers to a product that delivers nutrients to crops when i) encapsulated inside nanomaterials, such as a nanoporous network, or ii) coated with a thin polymer film, or iii) delivered as particles or emulsions of nanoscale dimensions. One of the most studied and promising inorganic materials for nanofertilization are metal oxide nanoparticles (MO NPs),[14] such as iron, copper and zinc,[15,16] or those based on more exotic elements, such as cerium.[17] NPs based on metal oxides have been demonstrated to have a better uptake efficacy than their bulk counterpart, since the high surface/volume ratio allows better absorption within the plant tissue. Among their positive effects, there are resistance to abiotic stress, greater production of metabolites, increase of radical elongation and of net photosynthesis. For example, fertilization with copper oxide NPs leads to increased root length, leaf chlorophyll and berry sugar contents in tomatoes[18] and boosted enzyme activities in maize.[19] Moreover, CuO NPs exhibit antimycotic activity against *Fusarium oxysporum* sp. in watermelon plants.[20] However, to regulate the nutrient dose absorbed by plants and to reduce waste, it is necessary to manage the controlled release of the nanofertilizer.

In this paper, a novel nanocomposite of CuO NPs encapsulated in a biopolymeric shell, based on chitosan and sodium alginate, has been proposed. Thanks to their chemical structure and the presence of amino and hydroxyl groups, biopolymers can interact with MO NPs, protecting them from the environment and also preventing the leaching of the elements into the soil.[21,22] Herein, a particular class of physically cross-linked hydrogels is presented that are sensitive to pH and to other environmental factors, such as temperature and ionic strength, known as polyelectrolyte complexes (PECs).[23,24] These properties make them particularly interesting for the controlled release of encapsulated material. The formation of PEC nanoaggregates in solution is driven by strong coulombic interaction between two oppositely charged polymers (polyelectrolytes), together with the contribution of hydrophobic interactions. When the polymers interact, the small counter-ions bound to the polymer escape from the polymeric network into the solution. The generated entropy favours the self-assembly of polymeric nanoparticles. In particular, ion–ion interactions take place between the charged portions of the two polymers, in addition to the hydrogen bonding. In this work the chosen polyelectrolyte polymers were chitosan (CS) and alginate (ALG). CS is a derivative of chitin and the most abundant natural polymer in the world after cellulose,[25] while ALG, a polyanion polymer, is a negatively charged polysaccharide consisting of 1 → 4 linked β-D-mannuronic acid and α-L-guluronic acid, derived from brown algae, such as kelp algae (order Laminariales). The ionic bonds between CS protonated amine residues and ALG carboxylic residues are responsible for PEC nanoparticle formation. Furthermore, the presence of hydroxylic, amino and carboxylic groups permits the two polymers to interact *via* hydrogen bonding (*i.e.* ion–dipole and dipole–dipole interactions).[26] However, although CS, CS-based hybrid nanocomposites and CS/ALG have been used as smart delivery systems in different application fields from medicine to sensors,[27–31] and CS is also a good candidate for application in agriculture[32] as a result of its beneficial effects on plant growth,[20,33,34] there are very few papers that report on the application of CS/ALG in agriculture.[35,36] Moreover, to the best of our knowledge there are no papers on hybrid nanocomposites made from CS/ALG and inorganic NPs.

Here, the proposed hybrid nanocomposite made from CuO and PEC NPs combines the known positive effects of CuO on plant growth and development, and the benefits of the biopolymer shell, which slows nutrient release. This approach also permits better adhesion of this material to the leaf surface by enabling the prolonged presence of copper cations, thus obtaining better nutrient use efficiency. The environmentally friendly preparation of the CuO/PEC hybrid nanocomposite is reported in detail. Structural investigation is carried out, in order to demonstrate the morphology and the chemical structure of the hybrid nanocomposite. Finally, the influence of the material on the germination of *Fortunella margarita* Swingle (kumquat tree) seeds, belonging to the *Rutaceae* family, the genus of which is related to the most

important *Citrus* spp. is evaluated. Also, the effects of different concentrations of the novel hybrid treatment on germination are taken into account.

Experimental

Materials

Chitosan (with low molecular weight and >75% *N*-deacetylation) and alginic acid sodium salt were procured from Sigma-Aldrich. Sodium tripolyphosphate (STPP) was supplied by Acros Organics. Copper(II) oxide nanopowder (30–50 nm particle size, 99% purity) was purchased from Alfa Aesar.

Preparation

PEC NPs were prepared according to the method proposed by Goycoolea *et al.*, with some slight modifications.[37] CS (1.0 mg ml^{-1}) was fully dissolved into 5 ml of acetate buffer (0.1 M, pH = 5.2) under magnetic stirring (1000 RPM) for about 1 h at room temperature. Deionized Milli-Q water was used in all the experiments. A 1 ml solution of STPP (1.0 mg ml^{-1}) was mixed with a 1 ml alginate solution (0.45 mg ml^{-1}), in order to obtain CS : STPP and CS : ALG ratios respectively equal to 5 : 1 and 11 : 1. Both solutions were prepared in the same 0.1 M acetate buffer, to guarantee constant pH during the subsequent preparation steps. Upon the mixing of the STPP-ALG solution (1 ml min^{-1}) into the CS solution kept under magnetic stirring (750 rpm) at room temperature, PEC NPs were spontaneously formed. Agitation was maintained for a further 30 minutes, in order to assure optimal dispersion of nanoparticles.

In order to realize a CuO/PEC nanocomposite, CuO nanopowder was dissolved in CS solution (1.0 mg ml^{-1}) under ultrasound treatment (50 kHz) for 15 minutes to obtain a well-dispersed suspension. Then, after stirring the suspension for 30 min, STPP-ALG solution was added to the CS-CuO solution using the same procedure used for the PEC NP preparation. The optimized CuO concentration was 100 ppm in the final suspension.

Methods

Thermal analysis. Thermogravimetric analyses (TGA) of both PEC and the CuO/PEC nanoparticles were performed using thermogravimetric apparatus (TA Instruments Q500) under a nitrogen flow (gas flow: 40 ml min^{-1} at 10 °C min^{-1} heating rate, up to 800 °C). PEC and CuO/PEC suspensions were centrifuged at 22 000 g for 30 minutes. The resulting pellet at the bottom of the vial was gently washed with water to remove excess salts and was dried in a vacuum oven at 60 °C for 48 h. A quantity of about 6 mg of the dried samples was used for TGA, where samples were weighed at room temperature. After an equilibration step carried out at 50 °C for 60 minutes, the weight loss percentage was recorded as a function of temperature.

X-ray diffraction (XRD). X-ray Diffraction (XRD) analysis of the CuO/PEC nanocomposite was performed using a Bruker-AXS D5005 θ–θ diffractometer equipped with a Cu Kα radiation source, operating at 40 kV and 30 mA in grazing incidence configuration. In order to perform the analysis, the CuO/PEC suspension was centrifuged at 22 000 g for 30 minutes to allow nanocomposite sedimentation on the vial bottom. Thus, the solid precipitate, separated from the water solution, was placed on Si slides using a micropipette and dried overnight prior to measurements being carried out.

Fourier-transform infrared (FTIR) spectroscopy. Fourier-transform infrared (FTIR) spectroscopy was performed on the CuO/PEC nanocomposite and PEC NPs after freeze-drying. Spectra were acquired in the 400–4000 cm^{-1} range using a PerkinElmer Spectrum 1000 spectrometer.

Dynamic light scattering (DLS). Dynamic light scattering (DLS) measurements were performed using homemade apparatus comprising a quartz scattering cell, confocal collecting optics, a Hamamatsu photomultiplier mounted on a rotating arm, a BI-9100 AT hardware correlator (Brookhaven Instruments Corporation) and a 660 nm diode laser. The laser power ranged between 5 and 50 mW. The auto-correlation function was provided by the hardware correlator operating in single photon counting regime.[38] We also evaluated the intensity distribution of the samples using a multi-exponential fitting procedure.

Electron microscopy. Electron Microscopy analysis was performed using scanning electron microscopy (SEM) and transmission electron microscopy (TEM). The SEM apparatus, ZEISS Supra 25, was equipped with an EDAX PV7715/89-ME energy dispersive X-ray (EDX) spectrometer for elemental characterization. For conventional morphological SEM analyses, the nanocomposite dispersion was drop cast onto a piece of silicon wafer and dried overnight at room temperature prior to analyses being carried out. The applied electron beam voltage was lowered to 5 keV to avoid charging effects and polymer modifications during image acquisition. For the EDX characterization, in order to avoid X-ray contribution from the underlying Si wafer, TEM 300 mesh nickel or golden grids were used. They were firstly dip coated into a dispersion of PEC and CuO/PEC nanocomposites, respectively, and then installed on a 6-sample carousel, conventionally conceived for TSEM (transmission SEM). For EDX maps, the operating voltage and the working distance were set to 25 keV and 8.5 mm respectively, to optimize the X-ray detection efficiency. TEM analyses were performed on JEOL JEM 2010F apparatus, operating at 200 keV.

Inductively coupled plasma optical emission spectrometry (ICP-OES). In order to evaluate the nanocomposite efficacy to bind the analyte and to delay its release, an *in vitro* dissolution test was performed using ICP-OES (Optima 2000 DV, PerkinElmer). The Cu release from the CuO/PEC nanocomposite and, as a reference, from CuO nanopowder dissolved in the same proportions in water was evaluated. Thus, 5 mg of both samples were placed in a 50 ml solution of 0.1 acetate buffer, at pH = 5.5. This value permits the

simulation of the acidic environment of the rhizosphere, which influences the availability of the essential elements and their absorption by the plants. Aliquots of 1.5 ml of both solutions were collected on days 0, 1, 2, 3, 4, 5, 7, 11, 14, and 22 (three replicates for each solution), then replaced by an equal volume of water and centrifuged at 22 000 *g* for 30 minutes. Then, 1.3 ml of supernatant were stored in vials, and a 400 μl aliquot was placed in 25 ml of a 1% HNO_3 solution to be analysed using ICP-OES.

Firstly, the calibration curve was set. Using a 1000 ppm ICP multi-elemental standard solution VI (Merck, Darmstadt, Germany), Cu-standard solutions were prepared at concentrations of 0.10, 0.25, 0.50, 1.00, 1.50, 2.00, and 2.50 ppm, and stabilized with the addition of 1% HNO_3. The reproducibility of the calibration curve was tested. Three calibration curves were obtained for the same solutions at three different emission lines for Cu (224.700, 324.752, and 327.393 nm) for each day of analysis.

Thus, for both samples, CuO and CuO/PEC, on all of the fixed days the release rate was calculated as the ratio between the measured Cu concentration and the total amount of Cu in the prepared solutions.

Germination assay

In laboratory, the efficacy of the nanocomposite as a seed germination promoter was tested. The research was conducted on *Fortunella margarita* Swingle. This species was chosen since, compared to the *Citrus* spp., its seeds are monoclonal, thus the risk of germination of non-zygotic plants during the trial was avoided. Seeds were extracted from fresh fruits and air-dried for 5 days in the laboratory. They were subsequently immersed in a 1% sodium hypochlorite solution for 30 minutes, under magnetic agitation, to ensure tegument sterility. Then, they were rinsed three times with distilled water, 15 minutes per rinse. Filter paper was put into a 100 mm × 15 mm Petri dish, and 8 ml of distilled water were added. Seeds were transferred above the filter paper, with 10 seeds per dish at a distance of 1 cm. Thus, the seeds were treated with 3 ml of treatment, and each treatment was repeated for three replicates. The used treatments were: CuO nanopowder at three concentrations, i) 10 ppm (CuO-10), ii) 50 ppm (CuO-50) and iii) 100 ppm (CuO-100); CuO/PEC solution at three concentrations, iv) 10 ppm (CuO/PEC-10), v) 50 ppm (CuO/PEC-50) and vi) 100 ppm (CuO/PEC-100); and two controls were used, vii) water and viii) only PEC solution. Petri dishes, covered and sealed using parafilm, were stored in a climatic chamber at 25 ± 0.1 °C in the dark. After incubation, the germination phases were followed for 31 days, when the seeds not yet germinated were moldy or dead for all the treatments. The emergence of radicles (the embryonic roots) and plumules (the embryonic shoots) was recorded on the following days (in hours) after incubation: 7 (168), 14 (336), 15 (360), 18 (432), 23 (552), 25 (600), and 31 (744). A spreadsheet was organized as suggested by Ranal *et al.*,[39] in order to evaluate the main germination parameters: germination percentage (*G*), mean germination time (*t*), coefficient of the variation of the germination time (CVt), mean germination rate (*v*), uncertainty (*U*), and synchrony (*Z*). In addition, the Vigor index (VI) was calculated as the product of germination (in %) and seedling length (in cm). The germination data were subjected to statistical analysis. Once the null hypothesis was rejected in the analysis of variance, we applied the Duncan test at 95% confidence interval. Finally, on day 31 the shoot development in seedlings, the root elongation and the presence of the secondary roots were registered.

Results and discussion

In order to obtain the nano formulated hybrid system of CuO/biopolymer with a low-cost production of nanoparticles, an eco-sustainable and green preparation method was selected. This avoids commonly used emulsion or precipitation methods, that require organic solvents, together with the use of high temperatures during the synthetic step.[40,41] As reported in literature by Goycoolea *et al.*,[37] by adding the STTP/ALG solution to the CS solution, the self-assembly of nanoparticles occurred spontaneously through the ionic gelation of CS–STTP and the concomitant complexation of the polyelectrolyte with ALG. In more detail, the process was regulated by the concomitant ionic cross-linking of CS to TPP, driven by the cross-linking between the negatively charged groups of STPP, the $P_3O_{10}^{5-}$ and $HP_3O_{10}^{4}$ ionic species, and a fraction of the positively charged amino groups of CS, $-NH_3^+$ groups, and the formation of an electrostatic complex between alginate carboxylic groups and chitosan amine groups. By adjusting the main synthesis parameters that regulate the solution ionic strength, such as pH, CS : ALG ratio and STPP amount, a stable solution of PEC nanoaggregates can be obtained.

When the CuO nanopowder was introduced in the CS solution, the polymeric chains easily bonded to the Cu cations owing to electrostatic interactions (*e.g.* hydrogen–ion bonding) between the metal oxide surface and the high number of functional amine ($-NH_2$) and hydroxyl (–OH) groups of CS.[42,43] The further addition of STPP guaranteed an extra linkage. As suggested by Koukaras *et al.*, the CS molecules were cross-linked to each other by STPP polyanions, thanks to the strong ionic interactions between the positively protonated polymeric amino and the negatively charged phosphate groups.[44] Finally, the carboxylic groups of ALG interacted with the residual positive sites of CS, wrapping all the previous layers.[27,45] Thus, a coating of PEC, made of CS, STTP and ALG, was able to envelop the CuO NPs. A scheme of the used flowchart and of the hybrid structure formulated in this work with a photograph of the nanocomposite are reported in Fig. 1.

The thermogravimetric analyses of both PEC and CuO/PEC nanoparticles were performed to obtain thermal behaviour of the samples, but also to gain quantitative information on the CuO residue and chemical composition.

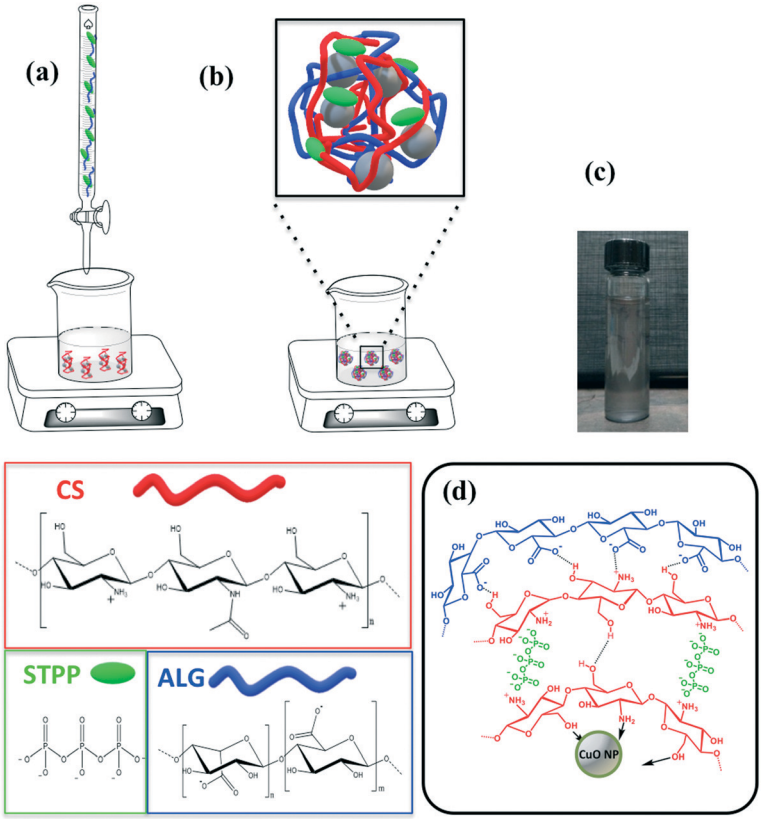

Fig. 1 (a) and (b) Schematic of the preparation of the CuO/PEC nanocomposite with a scheme of its chemical structure; (c) photograph of the CuO/PEC solution; (d) scheme of the CuO/PEC structure and interactions.

PEC nanoparticles presented complex thermograms characterized by different degradation steps, as evident from the TGA (shown in Fig. 2(a)) and DTG (derivative thermogravimetric) profiles (Fig. S1†). Although materials were kept in a vacuum oven at 60 °C for 2 days, an initial weight loss (up to 3% at 100 °C for CuO/PEC), due to residual water evaporation, was registered for both samples. This trend is reasonable due to the high hydrophilicity of the materials, as reported by Castelló *et al.*[46] At a higher temperature, several degradation phenomena caused by the decomposition of both alginate and chitosan components took place. The weight loss in the range 200–360 °C was due to chitosan and alginate degradation and carbonization. Specifically, this range is linked to the dehydration of the saccharide rings, depolymerization, and decomposition of the polymer units.[47,48] The weight loss at temperatures higher than 360 °C was attributed to the release of CH_4 due to a further dehydrogenation mechanism, which includes alginate decomposition to form Na_2CO_3. The final step at T >700 °C corresponded to the initial decomposition of Na_2CO_3, which contributed to the formation of residue (*ca.* 32 wt%) at 800 °C. The TGA curve of the CuO/PEC nanocomposite revealed that the presence of CuO nanoparticles showed a slight decrease in the degradation temperatures of the material, most likely due to the occurrence of a catalytic effect induced by the metal oxide. The polymer decomposition step at a higher temperature (>700 °C) was not appreciable due to the measurement sensitivity. Indeed, the residue registered for this sample corresponded to around 60%, revealing a metal oxide content of around 30% if compared with the unloaded samples.

The chemical interactions between the biopolymer and CuO were investigated by carrying out FTIR analysis on the PEC and CuO/PEC NPs. Although the acquired spectra, compared in Fig. 2(b), appear to be similar, there are some noticeable differences. Firstly, the PEC spectrum reveals a well-defined typical broad band in the 3600–3000 cm^{-1} spectral window,[49] corresponding to the stretching vibrations of –OH and $-NH_2$. Instead, in the CuO/PEC spectrum, sharper peaks at 3412, 3277 and 3164 cm^{-1} characterize this band, indicating some possible interactions between the polymeric –OH and $-NH_2$ groups and the CuO NP surface.[50] This point is also supported by the further appearance of new bands in the spectrum of the CuO/PEC at around 1690 cm^{-1}, which are usually attributed to the C=N stretching of amide vibrations.[51] In particular, the vibration at 1637 cm^{-1} was assigned to the modified amide I stretching of chitosan, ascribed to the strong interactions between the metal oxide and polymer ($-NHCOCH_3$) groups. In the CuO/PEC spectrum, a slight red shift can be observed at 1542 cm^{-1}, attributed to (COO–) stretching, compared to the 1557 cm^{-1} position in the PEC spectrum, as well as at 1338 cm^{-1} *versus* 1342 cm^{-1},

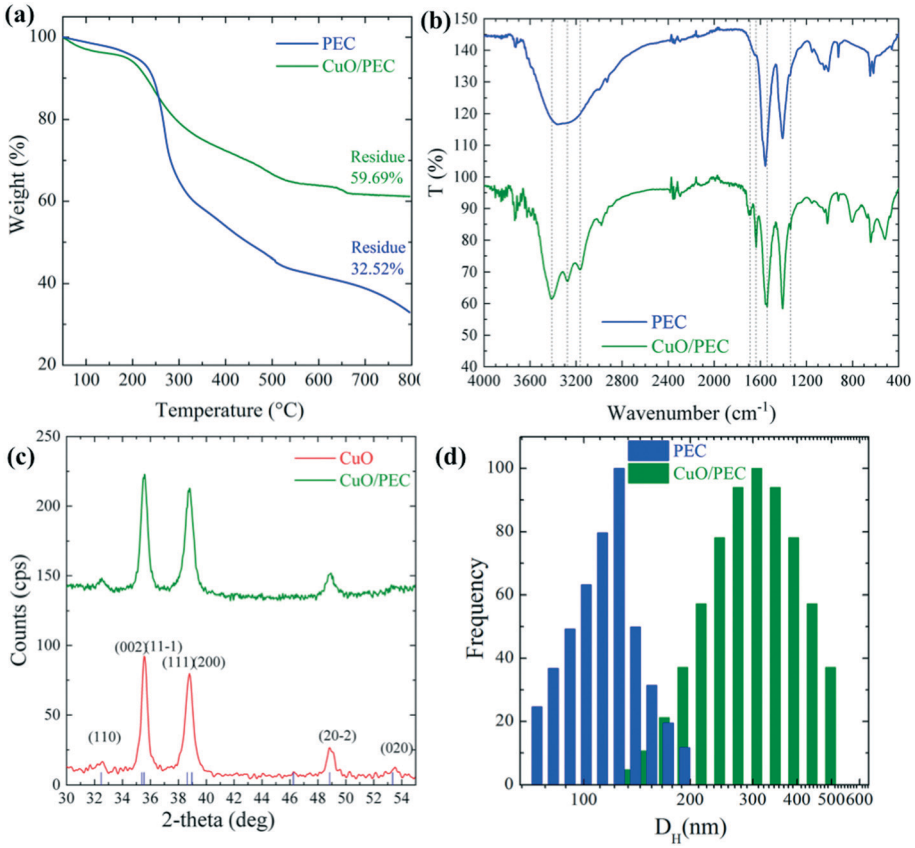

Fig. 2 (a) Thermogravimetric profiles of the PEC (blue trace) and CuO/PEC (green trace) samples. (b) Fourier-transform infrared spectra of PEC and CuO/PEC. Dashed lines refer to peaks indicative of the CuO/PEC complex formation. (c) X-ray diffraction patterns of the CuO/PEC and CuO nanopowder. The indexed peaks for the monoclinic CuO lattice are reported [JCPDS no. 41-0254]. (d) Hydrodynamic diameter, D_H, distributions for the PEC and CuO/PEC samples.

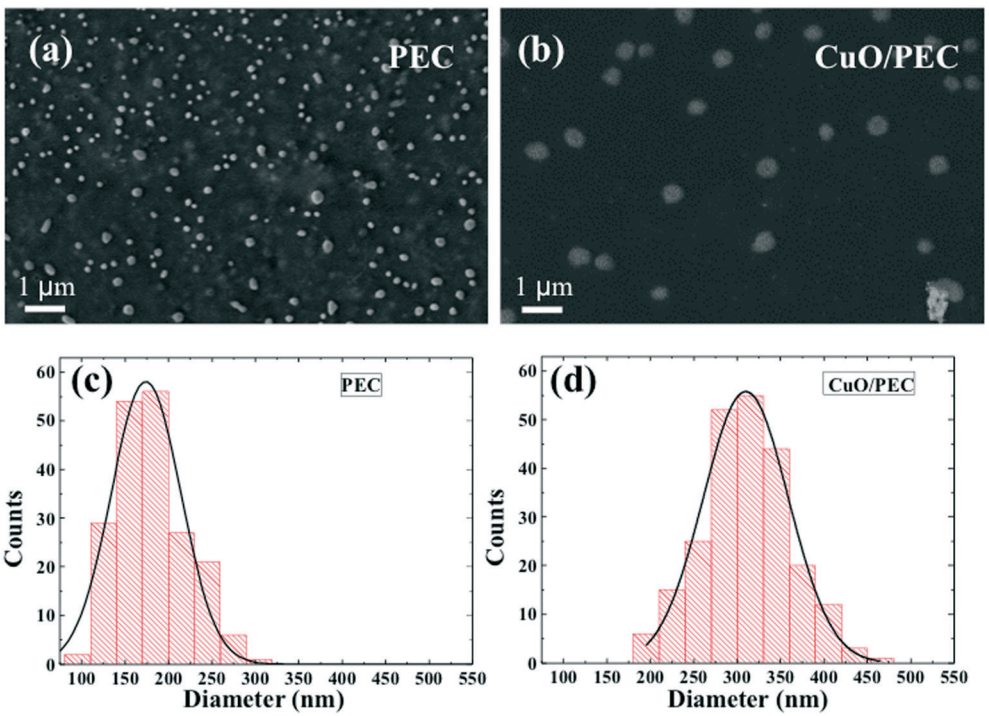

Fig. 3 Scanning electron microscopy images of (a) PEC and (b) CuO/PEC. The diameter distributions and the relative Gaussian fits for the (c) PEC and (d) CuO/PEC NPs.

associated with the chain skeleton vibration.[51] Furthermore, the bands near to 1070 cm^{-1}, usually attributed to the C–O and C–N stretching vibrations, appear sharper in the spectrum of the CuO/PEC, indicating that the C–O and C–N groups are also involved in metal coordination.[50] The peak at 923 cm^{-1} can be attributed to the P–O–P stretching.[52] Finally, in the CuO/PEC spectrum the new band in the 520 cm^{-1} range is often attributed to the stretching vibrations of N–CuO and O–CuO.[50,51,53,54] In conclusion, the FTIR data, herein reported, reveal the existence of ion–ion and ion–dipole interactions and hydrogen bonding between the ions pairs on the amide groups, the negatively charged carboxylic group, the positively charged amino groups, and the hydroxylic groups with atoms on the CuO NP surface. Thus, these results demonstrate the formulation of a CuO/PEC complex formed by polyelectrolyte complexation and therefore the effective incorporation of CuO inside the biopolymer.

Further support from XRD measurements revealed the presence of crystalline CuO in the CuO/PEC preparation. As visible in Fig. 2(c), the XRD pattern measured for the CuO/PEC nanocomposite appears identical to the pattern acquired for the commercial CuO nanopowder, the main diffraction peaks of which are indexed in the same figure. Any diffraction peaks relative to the biopolymer were not observed in the detection range.

DLS experiments were performed in order to obtain the hydrodynamic diameter (D_H) and the relative particle polydispersity for the PEC and CuO/PEC samples. The obtained correlation function showed the presence of two families of particles for both nanocomposites. The larger sized one, in the order of microns, was associated with very few (less than 0.01%) large aggregates present in solution, thus it was not further analyzed. Instead, the hydrodynamic diameter, D_H, distributions of the smaller particles, representative of the samples, are compared in Fig. 2(d). They show peaks at 122 and 317 nm with standard deviations of 25 and 95 nm for the PEC and CuO/PEC samples, respectively. Moreover, the polydispersity indices of the diameters (defined as the normalised variance of the diameter distribution) were estimated to be 0.04 and 0.09, respectively. The estimated values of polydispersity confirmed the goodness of the produced nanoparticles and the uniformity of the samples.[55]

The morphologies of both the PEC and CuO/PEC were analysed by SEM and TEM. SEM images are reported in Fig. 3(a) and (b) for PEC and CuO/PEC, respectively. All of the collected images show the formation of a high density of well-defined spherical NPs for the two samples. This evidence demonstrates the efficacy of the used preparation to induce the agglomeration of well separated nanostructures, also during the introduction of the CuO nanopowder.

Several plan view SEM images were analysed using the ImageJ software, in order to evaluate the distribution of the nanoparticle diameter, d, for both preparations. The distributions and the relative Gaussian fits are reported in Fig. 3(c) and (d) for PEC and CuO/PEC, respectively. It is

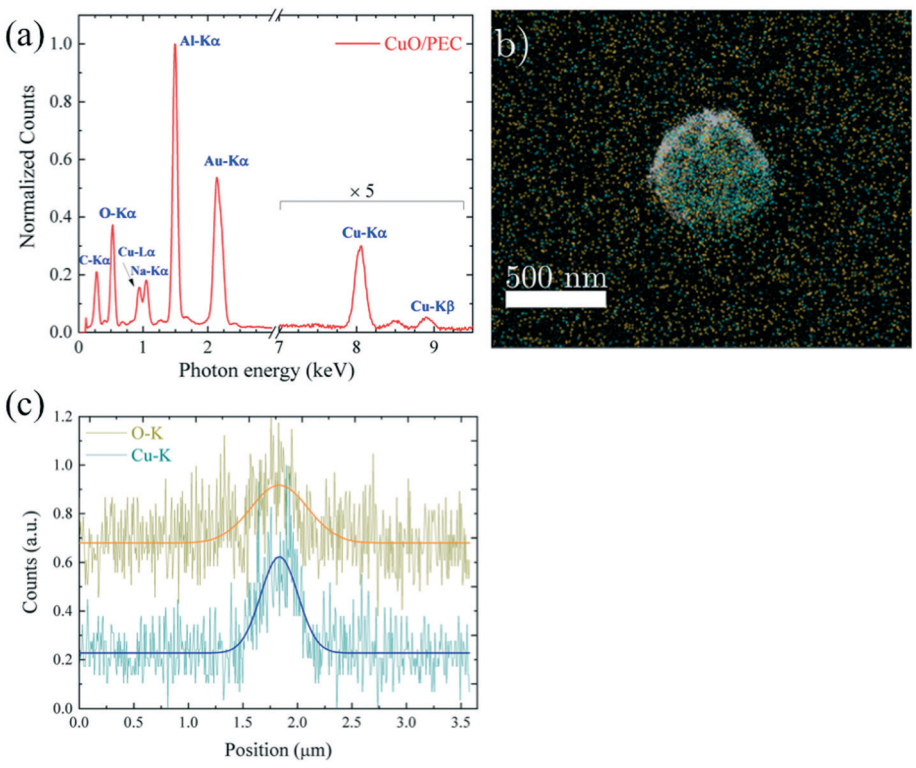

Fig. 4 (a) EDX spectrum of a CuO/PEC nanoparticle dried on an Au grid; (b) TSEM micrograph of a single CuO/PEC nanoparticle superimposed on a combined EDX map of O–K (dark yellow) and Cu–K shells (light blue); (c) intensity line profiles of Cu and O along the diameter of a CuO/PEC NP with the relative Gaussian fits.

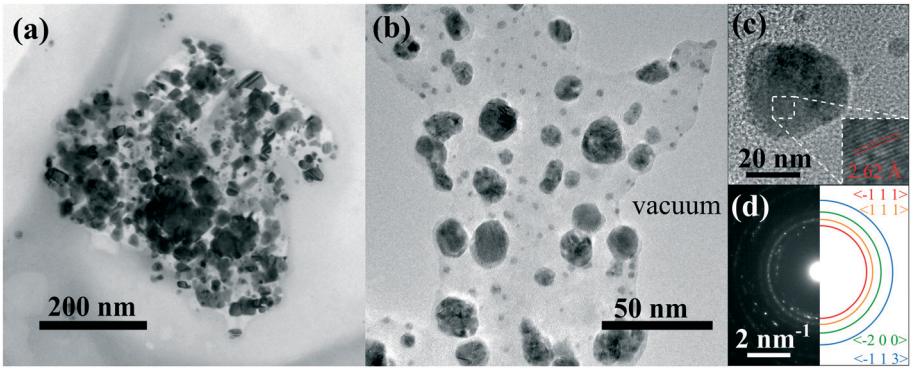

Fig. 5 (a) Bright field TEM image of an agglomeration of well separated nanostructures. (b) Higher magnification of a portion of CuO nanoparticles in the PEC matrix. (c) HR-TEM of a copper oxide nanoparticle. (d) Left: SAED of a portion of the nanoparticle. Right: Sketch of some diffraction rings, the interplanar spacings of which are in agreement with theory.[56]

noteworthy to observe the increased diameter of the CuO/PEC NPs, 309 ± 56 nm, compared with that of the PEC NPs, 174 ± 40 nm. The obtained values are compatible with the hydrodynamic diameters estimated by DLS (122 nm for PEC and 317 nm for CuO/PEC), which further suggests that the CuO NPs were incorporated inside the polymeric nanostructures.

To evaluate the spatial distribution of the metal oxide inside the biopolymer nanoparticles, EDX chemical mapping was performed on both samples, by working in TSEM (transmission SEM) mode. A micrograph for a single PEC NP is reported in Fig. S2(a)† and is superimposed with the elemental EDX maps relative to the O-K (yellow) and P-K (purple) signals acquired from the same nanoparticle in Fig. S2(b).† In all the area of the PEC NP, the O signal, associated with the PEC polymeric chains, is uniform, together with the P signal due to the STPP linker, which indicates spontaneous polymer nanoaggregation. These data further confirm the polymeric nature of the nanoparticles observed in the micrographs.

The analysis of the hybrid CuO/PEC nanocomposite reveals the presence of Cu, as demonstrated by the appearance of the Cu-Lα peak, detected at 0.930 eV, and the Cu Kα and Kβ peaks, in the energy range between 8.0 and 9.0 keV, in the EDX spectrum, reported in Fig. 4(a). The other observed peaks are associated with C (C-Kα at 0.277 keV), O (O-Kα at 0.525 keV) and Na (Na-Kα at 1.041 keV) relative to the two polymers, whereas Au (Au-Lα at 2.120 keV) is derived from the grid used as a support. Thus, the EDX elemental maps, acquired from a single CuO/PEC NP, allowed localization of the metal oxide, by superimposing the EDX elemental maps obtained by the O–K signal (fingerprint of both polymers, in yellow) and the Cu–K signal (fingerprint of the CuO nanopowders, in green) with the corresponding TSEM image, as shown in Fig. 4(b). The good matching between the O map and the NP morphology further corroborates the polymeric nature of the observed NP for the hybrid nanocomposite preparation. Moreover, from the comparison of the intensity line profiles relative to the O and Cu signals, recorded along the NP diameter and shown in Fig. 4(c), the O profile appears slightly larger than the one of Cu, indicating that the Cu-based nanostructure is well-embedded inside the polymer coating.

This assumption is also supported by TEM analyses, as visible in the bright field TEM image in Fig. 5(a), in which an ensemble of several dark nano-aggregates appears to be embedded inside a polymeric nanostructure of around 400 nm in size. The detailed CuO/PEC nanostructure is reported in Fig. 5(b), in which the nanopowder appears to be clearly embedded in the polymer matrix and the contours of the hybrid nanocomposite are clearly distinguishable. The high-resolution TEM (HR-TEM) image of a single nanostructure confirmed that the dark nano-aggregates in Fig. 5(a) are CuO NPs. Indeed the observed fringes in the HR-TEM image in Fig. 5(c) corresponded to interplanar spacings of 2.62 ± 0.33 Å, that are equal to the theoretical CuO {−1 1 1} distances.[56] Selected area electron diffraction (SAED) analyses were also performed, as shown in Fig. 5(d), in which the coloured semicircle on the right side highlights the diffraction rings. The obtained interplanar distances are $d_{(-1\ 1\ 1)}$ = 2.52 Å, $d_{(1\ 1\ 1)}$ = 2.33 Å, $d_{(-2\ 0\ 0)}$ = 1.82 Å, $d_{(-1\ 1\ 3)}$ = 1.44 Å, in accordance with theory.[56]

In addition, it is interesting to note that no other metal oxide aggregates were observed when the CuO nanopowder was added into the solution. This further confirms the outstanding efficacy of CuO nanopowder incorporation inside the polymer nanostructures during the hybrid nanocomposite preparation.

The role of polymeric coating in the release of Cu ions from CuO/PEC NPs was evaluated by performing release experiments for a period of 22 days. Firstly, calibration curves were obtained for Cu at the three used emission lines (224.700, 324.752, and 327.393 nm), as shown in Fig. S3.† Thus, copper release was evaluated by comparing the results from the CuO/PEC nanocomposite with the ones from bare CuO nanopowder, used as a reference. Fig. 6(a) shows the cumulative percentage release of Cu ions from the solubilisation of the two samples in aqueous solution under mild acidic conditions (acetic buffer, pH = 5.5).

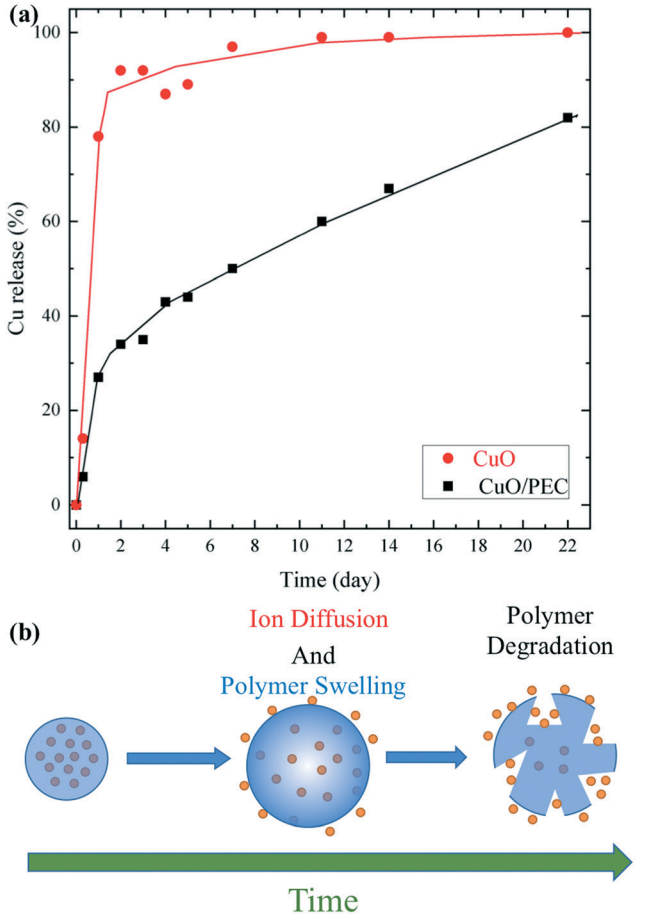

Fig. 6 (a) Cumulative percentage release of Cu *versus* time from CuO nanopowder and the CuO/PEC NPs, under a constant of pH = 5.5. (b) Schematic of the mechanism of Cu release from the CuO/PEC nanocomposite.

The red line indicates that the CuO NPs show a faster release of Cu ions in the solution during the first 2 days, reaching a percentage release of almost 90%, and the maximum on day 22. On the contrary, in the presence of the polymeric coating, the profile (black line) evidences a significantly slower Cu ion release. After 1 day of testing, the released of Cu was 3 times lower than from bare CuO nanoparticles. Upon an increase in the time, the Cu ion delivery from the CuO/PEC NPs continued to slowly increase, reaching 80% release after 22 days. This behaviour was reasonably attributed to the encapsulating action of the polymeric coating, which limited the rapid dissolution compared with that observed for bare CuO NPs in the used acidic medium. In addition, copper ions were linked to chitosan functional groups, characterized by their chelating capacity, which contributed to slow the Cu diffusion and release into the medium, as observed[57] for copper ions encapsulated in a CS porous network and for iron in iron oxide nanoparticles coated with CS.[58] Therefore, in the case of the CuO/PEC NPs, two main mechanisms can be hypothesized to describe the Cu release, Cu diffusion out of the polymeric nanoparticles, driven by the concentration gradient, and polymer swelling and degradation,[59,60] which took place over several days, as schematized in Fig. 6(b).

The information obtained herein can be proficiently used in the design of future slow-release nanofertilizers to mitigate metal ion accumulation in soil and plants.

Seed germination

The effects of three concentrations of CuO/PEC nanocomposite solution (10, 50 and 100 ppm) were tested on the germination of *Fortunella margarita* Swingle seeds. The same concentrations of CuO nanopowder were evaluated, as references, together with water and PEC controls. During the first days after incubation, the seeds grew by absorbing water and activating hydrolytic enzymes. The first evidence was the emergence of the radicles, the embryonic roots of the seedling. Then the radicles converted into roots and absorbed water and nutrients to supply the other parts of the plant. Secondly, a structure called a plumule emerged. The plumule is the embryonic part that forms the stem of the plant. In Fig. S4† the radicle (a) and plumule (b) emergence of the six treatments and the two controls are represented. The first radicle emission was observed after 14 days (336 h) from sowing for all the treatments, although each one was observed for a variable number of seeds. On day 14 the germination percentages were 43.4 for CuO/PEC_10, 36.7 for CuO/PEC_50 and water, 23.3 for CuO_10 and PEC, 16.7 for CuO/PEC_100 and CuO_50, 10.0 for CuO_100, as shown in Fig. 7(a). The main germination parameters (G, t, CVt, v, U, Z) measured on day 31 (344 h) are reported in Table S1.† By comparing all of the treatments, CuO/PEC_10 and CuO/PEC_50 showed the highest germination rates after 31 days, although without statistically significant differences.

In terms of plumules, the first emergences were observed on day 23 (400 h) from sowing, simultaneously in all treatments, but with differences in the number of seeds involved, as shown in Fig. S4.† The germination percentages were 26.7 for CuO/PEC_50, 16.7 for CuO/PEC_100, 13.3 for CuO/PEC_10 and PEC, 10.0 for CuO_50 and water, 6.7 for CuO_100 and 0.0 for CuO_10, as reported in Fig. 7(b). All the germination parameters obtained after 31 days are reported in Table S2.† Statistically significant differences emerged among the treatments only in terms of germination percentage. CuO/PEC_10 shows the highest rate of plumules emergence (80%), significant compared to water, PEC and CuO_10.

In terms of the vigor index both for radicles and plumules, the CuO/PEC_10 treatment showed the highest values, as evident in Fig. 7(c), which reports the calculated VI values for all the treatments and the controls. By further increasing the CuO/PEC concentration, we observed that for the radicle the CuO/PEC_100 treatment showed the worst performance, similar to the control water and to the CuO_10 treatment. Therefore, CuO/PEC_100 seemed to be a detrimental concentration also for the above-ground part of the seedling.

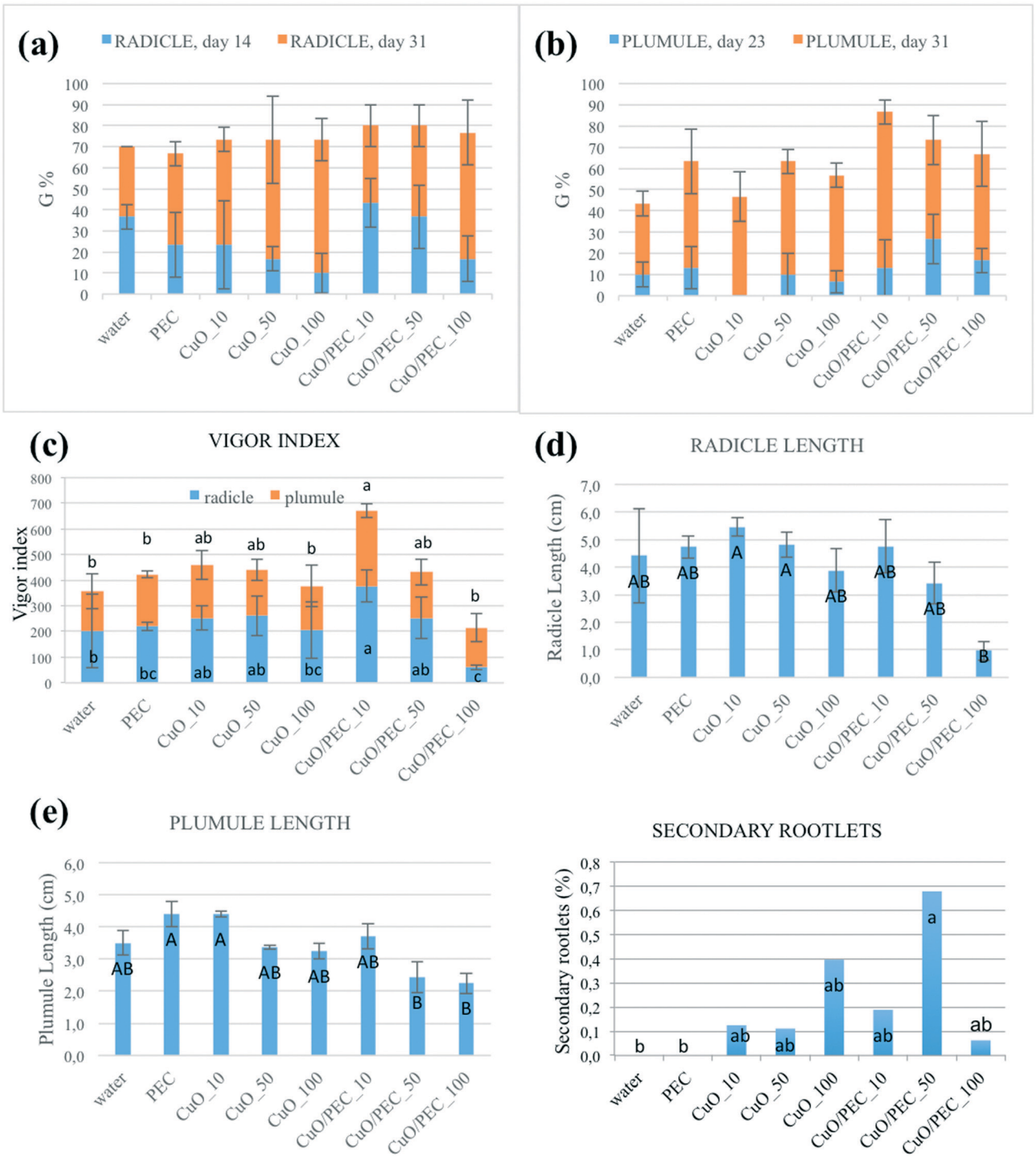

Fig. 7 Effects of the CuO/PEC NPs, at three different concentrations, on the germination percentage, *G*, of (a) radicles on days 14 and 31 and (b) plumule on days 14 and 31, on the (c) vigor index for both radicles and plumule on day 31, on (d) radicle and (e) plumule length on day 31. The effects of also CuO, at the same three concentrations, and only PEC and the water control are reported. Each value is the mean of triplicates, and each experiment consisted of 10 seedlings. Different letters indicate the significant differences among the treatments based on the Duncan test at $p \leq 0.05$ and $p \leq 0.01$ (lowercase and uppercase letters, respectively).

Finally, the radicle and plumule lengths were evaluated as, respectively, the distance from the root-shoot junction to the tip of the primary root and the vegetative apex. Both values together with the percentage of secondary rootlets are reported for all of the treatments in Table 1 and in Fig. 7(d)–(f).

By comparing all the data, the two control treatments, water and PEC, showed high values of root lengthening (hypogean part), but no development in secondary roots. In terms of the treatments, we observed that while CuO allowed a high development of the root (up to about 5.5 cm), but a

Table 1 Effect of the application of different concentrations of CuO and CuO/PEC solutions on *Fortunella margarita* Swingle seeds on radicle and plumule length, plumule/radicle ratio and development of secondary rootlets. Means followed by different letters in each column are significantly different based on the Duncan test at $p \leq 0.05$ and $p \leq 0.01$ (lowercase and uppercase letters, respectively)

Treatment	Radicle length (cm)		Plumule length (cm)		Plumule/radicle ratio		Secondary rootlets (%)	
Water	4.41 ± 1.71	AB	3.50 ± 0.38	AB	0.86 ± 0.27	B	0 ± 0	b
PEC	4.73 ± 0.40	AB	4.39 ± 0.39	A	0.93 ± 0.01	B	0 ± 0	b
CuO_10	5.46 ± 0.34	A	4.40 ± 0.10	A	0.81 ± 0.07	B	0.13 ± 0.18	ab
CuO_50	4.82 ± 0.46	A	3.38 ± 0.07	AB	0.70 ± 0.06	B	0.11 ± 0.19	ab
CuO_100	3.88 ± 0.78	AB	3.26 ± 0.25	AB	0.86 ± 0.13	B	0.40 ± 0.43	ab
CuO/PEC_10	4.76 ± 0.97	AB	3.70 ± 0.38	AB	0.79 ± 0.09	B	0.19 ± 0.20	ab
CuO/PEC_50	3.42 ± 0.75	AB	2.44 ± 0.48	B	0.72 ± 0.04	B	0.68 ± 0.36	a
CuO/PEC_100	0.96 ± 0.34	B	2.25 ± 0.32	B	2.64 ± 1.33	A	0.06 ± 0.09	ab

low development of secondary roots, instead the CuO/PEC treatments positively affected both germination and root elongation with a greater number of secondary roots observed. This result is of great interest, because it offers a better development of the shoots, the epigean part, as also evident in the photographs shown in Fig. 8, which show a comparison of the morphological characteristics of the seeds after each of the treatments and controls. Shoot development in seedlings is strongly linked to the reserved substances stored in the roots, while the development of the root as well as being related to the reserves of the cotyledons is also influenced by the physical and chemical characteristics of the growth substrate. Therefore, since the CuO/PEC treatment positively affected the development not only of the principal root (taproot) but also the secondary root emission, it ensures, in addition, a greater exploration of the growth substrate, thus improving the nutrient adsorption.

Concerning the dependence of germination on the metal oxide concentration, it was evident that CuO/PEC_10 and CuO/PEC_50 revealed the best root and shoot development balance with respect to the treatment at higher concentration, 100 ppm. Indeed, it is known that an excess of micronutrients becomes toxic, in particular, high Cu concentrations reduce root development, leading to deficient water and nutrient uptake and consequent growth reduction.[61,62] Eco-toxicity aspects are not the subject of investigation in this paper. Although NP toxicity strongly depends on the plant species, growth conditions, exposure time, concentration, type and size of NPs, we can assume that the concentration optimized for germination was in the range of low concentration that is reported in several works to not cause damage but to stimulate the plant growth by playing a crucial role as a microelement useful for the plant.[63–66]

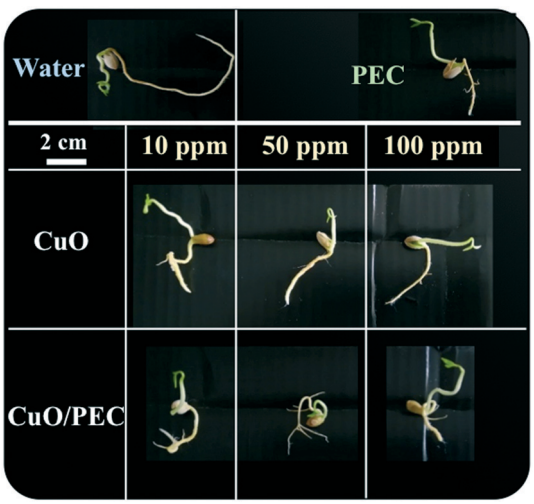

Fig. 8 Morphological characteristics of *Fortunella margarita* Swingle seeds after 30 days of treatment: in only water, PEC solution, CuO nanoparticles at 10 ppm, 50 ppm and 100 ppm, and CuO/PEC solution at 10 ppm, 50 ppm and 100 ppm.

Conclusions

Using an environmentally friendly approach, CuO NPs were successfully encapsulated inside PEC nanoparticles to obtain novel hybrid nanoparticles. DLS measurements gave information about their hydrodynamic diameter and the polydispersity index. Combined SEM and EDX analysis revealed that the as-performed synergic assembly of CS–ALG and STPP significantly influenced the nanoaggregrate formation, producing nanoparticles with a diameter of 174 ± 40 nm, which increased up to around 309 ± 56 nm after CuO incorporation. TEM analyses confirmed the hybrid nanocomposite structure, in particular, the HR-TEM image confirmed the crystalline nature of the CuO nano-aggregates inside the polymeric matrix. The interactions between the PEC functional groups and CuO were proved through the characterization of functional groups by FTIR analysis, whereas its presence was quantified by TGA, indicating a 30% metal core.

As tested by ICP-OES measurements, the synthesized hybrid CuO/PEC NPs showed ability to slow Cu release, where 80% copper release was achieved after 22 days compared with 1 day for bare CuO NPs. Finally, the nanocomposite also showed efficacy in increasing seed germination when applied on *Fortunella margarita* Swingle seeds.

Since the biodegradable coating reduces environmental impact, by slowing the release of the nanofertilizer, the novel CuO/PEC nanoformulation effectively acts as an efficient and eco-sustainable medium to regulate Cu fertilization without

dispersion in the soil. The latter property makes these materials attractive for the future design of slow-release nanofertilizers, specifically aimed at preventing their undesired accumulation in soil and plants. The results herein demonstrated are of great interest regarding the recent policy in agriculture, which recently saw the imposing of a strong reduction in Cu use in orchards.

Conflicts of interest

The authors declare no competing financial interests.

Acknowledgements

This work was funded by the ESF-Sicilia 2014-2020 call 11/2017 project SENTI (Sensori Elettronici, Nano Tecnologie, Informatica per l'agricoltura di precisione - CIP 2014.IT.05.SFOP.014/3/10.4/9.2.10/0007) coordinated by CNR-IVALSA. The authors want to thank A. Di Mauro for useful discussion, and C. Percolla and G. Pantè for expert technical assistance.

References

1 G. V. Lowry, A. Avellan and L. M. Gilbertson, Opportunities and challenges for nanotechnology in the agri-tech revolution, *Nat. Nanotechnol.*, 2019, **14**, 517–522.
2 R. Raliya, V. Saharan, C. Dimkpa and P. Biswas, Nanofertilizer for Precision and Sustainable Agriculture: Current State and Future Perspectives, *J. Agric. Food Chem.*, 2018, **66**, 6487–6503.
3 R. A. Wuana and F. E. Okieimen, Heavy Metals in Contaminated Soils: A Review of Sources, Chemistry, Risks and Best Available Strategies for Remediation, *ISRN Ecology*, 2011, 1–20.
4 P. Ahmad, in *Plant metal interaction: emerging remediation techniques*, ed. P. Ahmad, Elsevier, Amsterdam, 1st edn., 2016.
5 A. Verma and S. Bhatia, Analysis of some physicochemical parameters and trace metal concentration present in the soil around the area of Paricchа thernal power station in Jhansi, India, *Int. J. Innov. Res. Sci. Eng. Technol.*, 2014, **3**, 10482–10488.
6 A. Miotto, C. A. Ceretta, G. Brunetto, F. T. Nicoloso, E. Girotto, J. G. Farias, T. L. Tiecher, L. De Conti and G. Trentin, Copper uptake, accumulation and physiological changes in adult grapevines in response to excess copper in soil, *Plant Soil*, 2014, **374**, 593–610.
7 P. M. G. Nair and I. M. Chung, Study on the correlation between copper oxide nanoparticles induced growth suppression and enhanced lignification in Indian mustard (Brassica juncea L.), *Ecotoxicol. Environ. Saf.*, 2015, **113**, 302–313.
8 A. Aggarwal, I. Sharma, B. N. Tripathi, A. K. Munjal, M. Baunthiyal and V. Sharma, in Metal toxicity and photosynthesis, *Photosynthesis: Overview on recent progress and future perspectives*, ed. S. Itoh, P. Mohanty and K. N. Guruprasad, International Publishing House Limited, India, 2012, ch. 6, pp. 229–236.
9 D. E. Kopsell and D. A. Kopsell, In *Handbook of plant nutrition*, ed. A. V. Barker and D. J. Pilbeam, Taylor and Francis Group, New York, 2007, ch. 10, pp. 293–328.
10 K. Apel and H. Hirt, Reactive oxygen species: metabolism, oxidative stress and signal transduction, *Annu. Rev. Plant Biol.*, 2004, **55**, 373–399.
11 J. D. Mattos, O. C. Bataglia and J. A. Quaggio, in *Nutrição do citros*, ed. D. Mattos-Junior, J. S. Negri, R. M. Pio and P. J. J. Citros, Instituto Agronômico e Fundag, Campinas, 2005, pp. 198–219.
12 F. W. R. Hippler, R. M. Boaretto, J. A. Quaggio and D. Mattos Jr, Copper in Citrus production: required but avoided, *Citrus R&T*, 2017, **38**, 99–106.
13 M. C. Derosa, C. Monreal, M. Schnitzer, R. Walsh and Y. Sultan, Nanotechnology in fertilizers, *Nat. Nanotechnol.*, 2010, **5**, 91–91.
14 M. Kah, N. Tufenkji and J. C. White, Nano-enabled strategies to enhance crop nutrition and protection, *Nat. Nanotechnol.*, 2019, **14**, 532–540.
15 J. Lv, P. Christie and S. Zhang, Uptake, translocation, and transformation of metal-based nanoparticles in plants: recent advances and methodological challenges, *Environ. Sci.: Nano*, 2019, **6**, 41–59.
16 S. M. Savassa, *et al.*, Effects of ZnO Nanoparticles on Phaseolus vulgaris Germination and Seedling Development Determined by X-ray Spectroscopy, *ACS Appl. Nano Mater.*, 2018, **1**, 6414–6426.
17 H. Wu, N. Tito and J. P. Giraldo, Anionic Cerium Oxide Nanoparticles Protect Plant Photosynthesis from Abiotic Stress by Scavenging Reactive Oxygen Species, *ACS Nano*, 2017, **11**, 11283–11297.
18 W. H. Elmer and J. C. White, The use of metallic oxide nanoparticles to enhance growth of tomatoes and eggplants in disease infested soil or soilless medium, *Environ. Sci.: Nano*, 2016, **3**, 1072–1079.
19 T. Adhikari, D. Sarkar, H. Mashayekhi and B. Xing, Growth and enzymatic activity of maize (Zea mays L.) plant: Solution culture test for copper dioxide nano particles, *J. Plant Nutr.*, 2016, **39**, 99–115.
20 I. O. Adisa, *et al.* Recent advances in nano-enabled fertilizers and pesticides: A critical review of mechanisms of action, *Environ. Sci.: Nano*, 2019, **6**, 2002–2030.
21 J. S. Duhan, R. Kumar, N. Kumar, P. Kaur and K. Nehra, Nanotechnology: The new perspective in precision agriculture, *Biotechnol. Rep.*, 2017, **15**, 11–23.
22 K. Sampathkumar, K. X. Tan and S. C. J. Loo, Developing nano-delivery systems for agriculture and food applications with nature-derived polymers, *iScience*, 2020, **23**, 101055.
23 K. T. Delaney and G. H. Fredrickson, Theory of polyelectrolyte complexation - Complex coacervates are self-coacervates, *J. Chem. Phys.*, 2017, **146**, 224902.
24 J. P. Quiñones, H. Peniche and C. Peniche, Chitosan based self-assembled nanoparticles in drug delivery, *Polymer*, 2018, **10**, 1–32.

25 S. K. Shukla, A. K. Mishra, O. A. Arotiba and B. B. Mamba, Chitosan-based nanomaterials: A state-of-the-art review, *Int. J. Biol. Macromol.*, 2013, **59**, 46–58.

26 S. Boddohi, N. Moore, P. A. Johnson and M. J. Kipper, Polysaccharide-based polyelectrolyte complex nanoparticles from chitosan, heparin, and hyaluronan, *Biomacromolecules*, 2009, **10**, 1402–1409.

27 N. Kamaly, B. Yameen, J. Wu and O. C. Farokhzad, Degradable controlled-release polymers and polymeric nanoparticles: Mechanisms of controlling drug release, *Chem. Rev.*, 2016, **116**, 2602–2663.

28 S. Kumara, N. Chauhana, M. Gopalb, R. Kumarb and N. Dilbaghiaa, Development and evaluation of alginate–chitosan nanocapsules for controlled release of acetamiprid, *Int. J. Biol. Macromol.*, 2015, **81**, 631–637.

29 M. A. Azevedo, A. I. Bourbon, A. A. Vicente and M. A. Cerqueira, Alginate/chitosan nanoparticles for encapsulation and controlled release of vitamin B2, *Int. J. Biol. Macromol.*, 2014, **71**, 141–146.

30 L. Ge, M. Zhang, R. Wang, N. Li, L. Zhang, S. Liu and T. Jiao, Fabrication of CS/GA/RGO/Pd composite hydrogels for highly efficient catalytic reduction of organic pollutants, *RSC Adv.*, 2020, **10**, 15091–15097.

31 B. Ates, S. Koytepe, A. Ulu, C. Gurses and V. K. Thakur, Chemistry, structures, and Advanced Applications of Nanocomposites from Biorenewable Resources, *Chem. Rev.*, 2020, **120**, 9304–9362.

32 E. V. R. Campos, J. L. de Oliveira, L. F. Fraceto and B. Singh, Polysaccharides as safer release systems for agrochemicals, *Agron. Sustainable Dev.*, 2014, **35**, 47–66.

33 R. V. Kumaraswamy, S. Kumari, R. C. Choudhary, A. Pal, R. Raliya, P. Biswas and V. Saharan, Engineered chitosan based nanomaterials: Bioactivities, mechanisms and perspectives in plant protection and growth, *Int. J. Biol. Macromol.*, 2018, **113**, 494–506.

34 P. L. Kashyap, X. Xiang and P. Heiden, Chitosan nanoparticle based delivery systems for sustainable agriculture, *Int. J. Biol. Macromol.*, 2015, **77**, 36–51.

35 M. D. S. Silva, D. Sgarbi Cocenza, R. Grillo, N. Ferreira Silva de Melo, P. S. Tonello, L. Camargo de Oliveirac, D. L. Cassimirod, A. H. Rosaa and L. F. Fraceto, Paraquat-loaded alginate/chitosan nanoparticles: Preparation, characterization and soil sorption studies, *J. Hazard. Mater.*, 2011, **190**, 366–374.

36 L. Jianhua, J. Xiao, F. Li, Y. Shi, D. Li and Q. Huang, Chitosan-sodium alginate nanoparticle as a delivery system for ε-polylysine: Preparation, characterization and antimicrobial activity, *Food Control*, 2018, **91**, 302–310.

37 F. M. Goycoolea, G. Lollo, C. Remuñán-López, F. Quaglia and M. J. Alonso, Chitosan-alginate blended nanoparticles as carriers for the transmucosal delivery of macromolecules, *Biomacromolecules*, 2009, **10**, 1736–1743.

38 M. Zimbone, P. Musumeci, P. Baeri, E. Messina, S. Boninelli, G. Compagnini and L. Calcagno, Rotational dynamics of gold nanoparticle chains in water solution, *J. Nanopart. Res.*, 2012, **14**, 1308.

39 M. A. Ranal, D. Garcia de Santana, W. Resende Ferreira and C. Mendes-Rodrigues, Calculating germination measurements and organizing spreadsheets, *Rev. Bras. Bot.*, 2009, **32**, 849–855.

40 J. Berger, M. Reist, J. M. Mayer, O. Felt, N. A. Peppas and R. Gurny, Structure and interactions in covalently and ionically crosslinked chitosan hydrogels for biomedical applications, *Eur. J. Pharm. Biopharm.*, 2004, **57**, 19–34.

41 C. P. Reis, R. J. Neufeld, A. J. Ribeiro and F. Veiga, Nanoencapsulation I. Methods for preparation of drug-loaded polymeric nanoparticles, *Nanomed.: Nanotechnol., Biol. Med.*, 2006, **2**, 8–21.

42 G. Unsoy, S. Yalcin, R. Khodadust, G. Gunduz and U. Gunduz, Synthesis optimization and characterization of chitosan coated iron oxide nanoparticles produced for biomedical applications, *J. Nanopart. Res.*, 2012, **14**, 964.

43 M. Kaloti and A. Kumar, Synthesis of Chitosan-Mediated Silver Coated γ-Fe2O3 (Ag–γ-Fe2O3@Cs) Superparamagnetic Binary Nanohybrids for Multifunctional Applications, *J. Phys. Chem. C*, 2016, **120**, 17627–17644.

44 E. N. Koukaras, A. Papadimitriou, D. N. Bikiaris and G. E. Froudakis, Insight on the Formation of Chitosan Nanoparticles through Ionotropic Gelation with Tripolyphosphate, *Mol. Pharmaceutics*, 2012, **9**, 2856–2862.

45 F. L. Mi, H. W. Sung and S. S. Shyu, Drug release from chitosan-alginate complex beads reinforced by a naturally occurring cross-linking agent, *Carbohydr. Polym.*, 2002, **48**, 61–72.

46 J. Castelló, M. Gallardo, M. A. Busquetsa and J. Estelrich, Chitosan (or alginate)-coated iron oxide nanoparticles: A comparative study, *Colloids Surf., A*, 2015, **468**, 151–158.

47 A. T. Paulino, J. I. Simionato, J. C. Garcia and J. Nozaki, Characterization of chitosan and chitin produced from silkworm chrysalides, *Carbohydr. Polym.*, 2006, **64**, 98–103.

48 M. L. Tummino, G. Magnacca, D. Cimino, E. Laurenti and R. Nisticò, The Innovation Comes from the Sea: Chitosan and Alginate Hybrid Gels and Films as Sustainable Materials for Wastewater Remediation, *Int. J. Mol. Sci.*, 2020, **21**, 550.

49 D. Kulig, A. Zimoch-Korzycka, A. Jarmoluk and K. Marycz, Study on alginate-chitosan complex formed with different polymers ratio, *Polymer*, 2016, **8**, 1–17.

50 I. Perelshtein, *et al.*, Chitosan and chitosan–ZnO-based complex nanoparticles: formation, characterization, and antibacterial activity, *J. Mater. Chem. B*, 2013, **1**, 1968–1976.

51 Y. G. Kang, H. C. Vu, T. T. Le and Y. S. Chang, Activation of persulfate by a novel Fe(II)-immobilized chitosan/alginate composite for bisphenol A degradation, *Chem. Eng. J.*, 2018, **353**, 736–745.

52 D. França, Â. F. Medina, L. L. Messa, C. F. Souza and R. Faez, Chitosan spray-dried microcapsule and microsphere as fertilizer host for swellable – controlled release materials, *Carbohydr. Polym.*, 2018, **196**, 47–55.

53 G. Li, *et al.* Iron(II) cross-linked chitin-based gel beads: Preparation, magnetic property and adsorption of methyl orange, *Carbohydr. Polym.*, 2010, **82**, 706–713.

54 S. Farhoudian, M. Yadollahi and H. Namazi, Facile synthesis of antibacterial chitosan/CuO bio-nanocomposite hydrogel beads, *Int. J. Biol. Macromol.*, 2016, **82**, 837–843.
55 L. A. A. Neto, T. M. Pereira and L. P. Silva, Magnetic nanoparticles coated with carbohydrates for 3D culture of bacteria, *Mater. Sci. Eng., C*, 2020, **116**, 111267.
56 R. D. Heidenreich and K. H. Storks, Note on Electron Diffraction Patterns of CuO, *J. Appl. Phys.*, 1955, **26**, 1056.
57 R. C. Choudhary, *et al.*, Cu-chitosan nanoparticle boost defense responses and plant growth in maize (Zea mays L.), *Sci. Rep.*, 2017, **7**, 1–11.
58 B. Y. Chen, H. W. Kuo, V. K. Sharma and W. Den, Chitosan Encapsulation of Ferrate^{VI} for Controlled Release to Water: Mechanistic Insights and Degradation of Organic Contaminant, *Sci. Rep.*, 2019, **9**, 18268.
59 M. A. Mohammed, J. Syeda, K. M. Wasan and E. K. Wasan, An overview of chitosan nanoparticles and its application in non-parenteral drug delivery, *Pharmaceutics*, 2017, **9**, 53.
60 S. Shakiba, C. E. Astete, S. Paudel, C. M. Sabliov, D. F. Rodrigues and S. M. Louie, Emerging investigator series: polymeric nanocarriers for agricultural applications: synthesis, characterization, and environmental and biological interactions, *Environ. Sci.: Nano*, 2020, **7**, 37–67.
61 A. M. B. Pahlsson, Toxicity of heavy-metals (Zn, Cu, Cd, Pb) to vascular plants - a literature-review, *Water, Air, Soil Pollut.*, 1989, **47**, 287–319.
62 N. M. Duran, S. M. Savassa, R. Giovanini de Lima, E. de Almeida, F. S. Linhares, C. A. M. van Gestel and H. W. Pereira de Carvalho, X-ray Spectroscopy Uncovering the Effects of Cu Based Nanoparticle Concentration and Structure on Phaseolus vulgaris Germination and Seedling Development, *J. Agric. Food Chem.*, 2017, **65**, 7874–7884.
63 H. L. Karlsson, J. Gustafsson, P. Cronholm and L. Möller, Size-dependent toxicity of metal oxide particles—a comparison between nano- and micrometer size, *Toxicol. Lett.*, 2009, **188**, 112–118.
64 M. Wierzbicka and J. Obidzinska, The uptake of lead on seed imbibition and germination in different plant species, *Plant Sci.*, 1998, **137**, 155–171.
65 T. Adhikari, S. Kundu, A. K. Biswas, J. C. Tarafdar and A. S. Rao, Effect of Copper Oxide Nano Particle on Seed Germination of Selected Crops, *J. Agric. Sci. Technol. A*, 2012, **2**, 815–823.
66 M. Simonin, A. A. M. Cantarel, A. Crouzet, J. Gervaix, J. M. F. Martins and A. Richaume, Negative Effects of Copper Oxide Nanoparticles on Carbon and Nitrogen Cycle Microbial Activities in Contrasting Agricultural Soils and in Presence of Plants, *Front. Microbiol.*, 2018, **9**, 3102.